Identification of Highly Efficient Delay-Rational Macromodels of Long Interconnects from Tabulated Frequency Data

Identification of Highly Efficient Delay-Rational Macromodels of Long Interconnects From Tabulated Frequency Data

Piero Triverio, *Member, IEEE*, Stefano Grivet-Talocia, *Senior Member, IEEE*, and Alessandro Chinea

***Abstract*—We introduce a novel formulation of black-box models for long multiconductor interconnects, together with an identification algorithm from tabulated scattering parameters. The fundamental assumption requires a modal decomposition matrix that does not depend on frequency. The model structure includes low-order rational coefficients with suitable delay operators. The latter are included in a feedback loop; therefore, all infinite signal reflections are automatically accounted for. This feature may lead to significant speed up factors during circuit-based transient simulation with respect to other state-of-the-art solutions. The model is cast in a delayed descriptor form, leading to a straightforward conversion to an equivalent SPICE-compatible netlist. Finally, a purely algebraic stability test is presented based on a linear matrix inequality. The very high efficiency of the proposed models is demonstrated through several application examples.**

***Index Terms*—Delay extraction, descriptor systems, high-speed interconnects, macromodeling, rational approximation, scattering parameters, transmission lines.**

I. Introduction

ELECTRICAL interconnects constitute a major limiting factor for the performance of high-speed systems [1], [2]. Severe attenuation, dispersion, crosstalk, and other parasitic effects may indeed compromise the signal integrity of the overall system if not properly characterized and accounted for during the system design flow. The above problems become more and more prominent when the physical length of the interconnects and the signals bandwidth increase. Therefore, the availability of accurate and efficient interconnect models that are able to predict all relevant signal degradation phenomena is of paramount importance. These models must be compatible with standard circuit simulation environments, such as SPICE, enabling system-level transient simulations of the interconnect closed on nonlinear terminations like digital or mixed-signal devices.

This study focuses on the generation of black-box simulation models of electrically long interconnects starting from tabulated frequency responses in scattering form. These are usually obtained from direct measurements or from field-based characterizations. This process, usually called *macromodeling* [1], aims at extracting a SPICE-compatible netlist having a response matrix that matches the raw data with a prescribed accuracy.

Lumped macromodeling via vector fitting [3] or similar algorithms [4], [5] is now a standard practice for electrically short interconnects [1], [2], [6], as well as microwave devices [7]–[10]. A rational curve-fitting scheme based on iterative least squares solutions [3] is performed on the data, leading to a state-space model and to a straightforward SPICE synthesis [11]. Unfortunately, this approach fails when the electrical length of the interconnect is significant since an excessive number of pole/residue terms is needed to represent the fast phase variations induced by propagation delays. For this reason, several extensions have been proposed for an explicit inclusion of such propagation delays in the model structure [12]–[19].

The so-called delayed vector fitting [12], [13] expands the transfer matrix into a finite number of single-delay terms, each representing the response contribution coming from an individual signal reflection from internal or external discontinuities. Quite significant improvements in model efficiency have been demonstrated by delayed vector fitting with respect to purely rational macromodeling schemes [12], [13]. Unfortunately, the number of delay terms must be fixed *a priori* based on heuristic considerations. Increasing the number of such delays also inevitably leads to more complex and less efficient models.

In the case of structures with no internal discontinuities, such as transmission lines and cables, delay-rational models including delay operators in a feedback loop have been proposed in [14]. Such model structures can represent all infinite reflections from the (generally unmatched) terminations, leading to more compact and efficient models with respect to delayed vector fitting. Currently, this compact formulation is only available for scalar (two-port) interconnects [14]. The main objective of this study is to generalize these methods by applying a delay-rational approximation in the modal domain, thus allowing a consistent treatment of interconnects with multiple and generally different modal delays.

It should be noted that the presented approach shares the same objective of all delay-based macromodeling methods for frequency-dependent multiconductor transmission line structures such as ToPLine [20] or DEPACT [21]. However, these techniques require knowledge of the per-unit-length parameter matrices defining the electrical behavior of the structure via telegrapher's equations [2]. This information is not available here since we are interested in a purely black-box identification strategy able to process tabulated frequency responses possibly coming

Manuscript received July 10, 2009; revised November 24, 2009. First published February 05, 2010; current version published March 12, 2010. This work was supported in part by the Istituto Superiore Mario Boella (ISMB).

The authors are with the Department of Electronics, Politecnico di Torino, Turin 10129, Italy (e-mail: piero.triverio@polito.it; stefano.grivet@polito.it; alessandro.chinea@polito.it).

Color versions of one or more of the figures in this paper are available online at http://ieeexplore.ieee.org.

Digital Object Identifier 10.1109/TMTT.2010.2040349

from direct measurements. Another generalization of the proposed method is the applicability to structures with a nonuniform and smoothly varying cross section, as will be demonstrated by the numerical examples.

The main limitation of the proposed technique is on the structure of the interconnect modes of propagation. We explicitly require that these modes do not depend on frequency [2] or that they can be reasonably approximated by constant modal profiles. This limitation obviously restricts applicability of the approach. However, several classes of structures that are commonly employed for high-speed signaling can be modeled, including uniform or nonuniform interconnects characterized by some degree of symmetry in their cross section [2]. The generalization to the case of frequency-dependent modes will be subject for a future investigation.

II. Formulation

We consider an L-conductor interconnect characterized by its $2L \times 2L$ tabulated scattering matrix at several frequency points $\omega_1, \omega_2, \ldots, \omega_{\bar{k}}$. We denote these available samples as

$$\mathbf{H}_k \in \mathbb{C}^{2L \times 2L}, \qquad k = 1, \ldots, \bar{k}. \tag{1}$$

The near-end ports are numbered consecutively as $1, \ldots, L$, followed by the far-end ports $L+1, \ldots, 2L$. Emphasis is on electrically long structures with a much larger physical length than the wavelength associated to the propagating fields at the maximum modeling frequency. This condition is associated, in the time domain, to nonnegligible propagation delays of the signals traveling along the interconnect. The main objective of this paper is to devise a robust black-box identification technique for extracting a compact equivalent model by taking into account the presence of suitable delay operators in the model structure.

Due to the adopted port numbering scheme, we have the following block structure:

$$\mathbf{H}_k = \begin{bmatrix} \mathbf{H}_{11,k} & \mathbf{H}_{12,k} \\ \mathbf{H}_{21,k} & \mathbf{H}_{22,k} \end{bmatrix}, \qquad k = 1, \ldots, \bar{k} \tag{2}$$

where all blocks have size $L \times L$. We restrict our attention to those interconnects having propagation modes that do not depend on frequency. Although this assumption may seem overly restrictive, several cases of interest fall into this class, including balanced differential pairs or cyclic-symmetric lines (see Section II-A). Moreover, even if the modes are frequency dependent, excellent constant approximations may often be used with almost no impact on the model accuracy [22], as described in Section III-A. Therefore, we assume that there exists a constant orthonormal eigenvector matrix $\mathbf{R} \in \mathbb{R}^{L \times L}$ that diagonalizes simultaneously all four blocks in (2). Defining a global decomposition matrix $\mathbf{T} \in \mathbb{R}^{2L \times 2L}$ as

$$\mathbf{T} = \begin{bmatrix} \mathbf{R} & \mathbf{0} \\ \mathbf{0} & \mathbf{R} \end{bmatrix} \tag{3}$$

we obtain

$$\mathbf{H}'_k = \mathbf{T}^T \mathbf{H}_k \mathbf{T} = \begin{bmatrix} \mathbf{\Lambda}_{11,k} & \mathbf{\Lambda}_{12,k} \\ \mathbf{\Lambda}_{21,k} & \mathbf{\Lambda}_{22,k} \end{bmatrix} \tag{4}$$

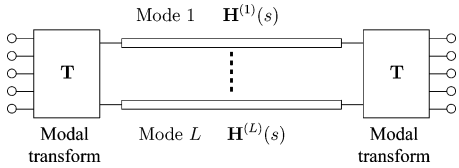

Fig. 1. Structure of the propose macromodel, composed by two modal transformation blocks and L macromodels $\mathbf{H}^{(l)}(s)$ representing modal lines.

where $\mathbf{\Lambda}_{ij,k} = \mathrm{diag}\{\lambda^{(1)}_{ij,k}, \ldots, \lambda^{(L)}_{ij,k}\}$ $i, j = 1, 2$. We will also consider cases where this diagonalization is not exact, as far as the off-diagonal terms in $\mathbf{\Lambda}_{ij,k}$ are sufficiently small to be neglected without significant loss of accuracy.

If we rearrange the rows and columns of $\mathbf{H}'_k$ with a suitable permutation matrix $\mathbf{P}$, we can make the original samples $\mathbf{H}_k$ block diagonal

$$\mathbf{H}''_k = \mathbf{P}^T \mathbf{H}'_k \mathbf{P} = \mathrm{blkdiag}\left\{\mathbf{H}^{(l)}_k\right\} \tag{5}$$

where each diagonal block has size 2×2 and reads

$$\mathbf{H}^{(l)}_k = \begin{bmatrix} \lambda^{(l)}_{11,k} & \lambda^{(l)}_{12,k} \\ \lambda^{(l)}_{21,k} & \lambda^{(l)}_{22,k} \end{bmatrix}, \qquad l = 1, \ldots, L. \tag{6}$$

This decomposition suggests the model structure shown in Fig. 1 with L modal lines and two modal transformation blocks. The modal lines will be represented by L macromodels $\mathbf{H}^{(l)}(s)$ identified from the samples (6), as discussed in Section III. Once all macromodels $\mathbf{H}^{(l)}(s)$ have been obtained, the global interconnect macromodel $\mathbf{H}(s)$ will read

$$\mathbf{H}(s) = \mathbf{T}\mathbf{P} \begin{bmatrix} \mathbf{H}^{(1)}(s) & & \\ & \ddots & \\ & & \mathbf{H}^{(L)}(s) \end{bmatrix} \mathbf{P}^T \mathbf{T}^T. \tag{7}$$

Reminiscent of the method of characteristics model for uniform transmission lines [2], [20], this structure inherits many of its properties, most notably the high computational efficiency.

Before proceeding any further, we highlight the differences between the adopted modal decomposition and [22]. In [22], the modal projection matrix (3) is full, meaning that the interconnect is treated as a generic $2L$-port with $2L$ modes excited by a combination of *both* near- and far-end signals. There is, therefore, no connection between such modes and the forward and backward propagating waves supported by the structure. This physical connection is instead retained in (7) due to the block-diagonal structure of matrix (3). Therefore, the interpretation of the proposed model in terms of the modal transmission lines (see Fig. 1) is straightforward. Only L modal macromodels are needed instead of $2L$, thus improving physical consistency and efficiency.

A. Cyclic-Symmetric Interconnects

An important case for which the diagonalization (4) holds with no approximations is provided by cyclic-symmetric interconnects [2]. These are formed by an arbitrary number L of identical conductors placed symmetrically with respect to a reference (return) conductor. The surrounding medium must be

symmetric and can possibly be inhomogeneous, as in the case of a set of wires with dielectric coating.

For cyclic-symmetric interconnects, each scattering matrix block in (2) is such that

$$\mathbf{H}_{ij,k} \in \mathsf{C}^{L\times L} \qquad \forall k \tag{8}$$

where $\mathsf{C}^{L\times L}$ is the set of complex-valued matrices of size $L\times L$ in the form

$$\mathbf{M} \in \mathsf{C} \Leftrightarrow \mathbf{M} = \begin{bmatrix} c_1 & c_2 & \cdots & c_3 & c_2 \\ c_2 & c_1 & \ddots & & c_3 \\ \vdots & \ddots & \ddots & \ddots & \vdots \\ c_3 & & \ddots & c_1 & c_2 \\ c_2 & c_3 & \cdots & c_2 & c_1 \end{bmatrix}. \tag{9}$$

These matrices are usually referred to as circulant symmetric matrices [23], [24]. Their eigenvalues are given by [23], [25]

$$\lambda^{(l)} = c_1 + c_2 v_l + c_3 v_l^2 + \ldots + c_3 v_l^{L-2} + c_2 v_l^{L-1} \tag{10}$$

where $v_l = \exp(j2\pi(l-1)/L)$ for $l = 1,\ldots,L$. Most of the eigenvalues (10) are double since we have

$$\lambda^{(l)} = \lambda^{(L+2-l)}, \qquad l = 2,\ldots,\nu \tag{11}$$

where

$$\nu = \begin{cases} (L+1)/2, & \text{if } L \text{ is odd} \\ L/2, & \text{if } L \text{ is even.} \end{cases} \tag{12}$$

Only $\lambda^{(1)}$ and, if L is even, also $\lambda^{(L/2+1)}$ are distinct.

Due to the coincident eigenvalues, the choice of an eigenvector matrix $\mathbf{R} \in \mathbb{R}^{L\times L}$ that diagonalizes $\mathbf{M}$

$$\mathbf{R}^T\mathbf{M}\mathbf{R} = \operatorname{diag}\{\lambda^{(l)}\}. \tag{13}$$

is not unique. Among the infinite choices of $\mathbf{R}$, we adopt the only one that is purely real [25], which is given by

$$\mathbf{R}_{m,1} = \sqrt{\frac{1}{L}} \tag{14a}$$

$$\mathbf{R}_{m,L/2+1} = \frac{(-1)^{(m-1)}}{\sqrt{L}} \quad \text{(only if } L \text{ is even)} \tag{14b}$$

$$\mathbf{R}_{m,l} = \sqrt{\frac{2}{L}} \cos\left[\frac{2\pi}{L}(m-1)(l-1)\right] \tag{14c}$$

$$\mathbf{R}_{m,L+2-l} = -\sqrt{\frac{2}{L}} \sin\left[\frac{2\pi}{L}(m-1)(l-1)\right] \tag{14d}$$

with $l = 2,\ldots,\nu$, $m = 1,\ldots,L$, and where $\mathbf{R}_{m,l}$ denotes the (m,l) entry of matrix $\mathbf{R}$. The realness of (14a)–(14d) is important for the macromodel synthesis in an equivalent electrical circuit (see Section IV). Other complex-valued choices [2] would make the synthesis procedure more difficult and are, therefore, avoided.

We finally note two properties of $\mathbf{R}$. First, $\mathbf{R}$ descends from the circulant symmetric structure of (9) and does not depend on the actual matrix entries. Second, $\mathbf{R}$ is an orthonormal matrix, i.e., $\mathbf{R}^T\mathbf{R} = \mathbf{R}\mathbf{R}^T = \mathbf{I}_L$, where $\mathbf{I}_L$ is the identity matrix of size $L \times L$.

B. Structure of Modal Macromodels

The formulation of modal macromodels $\mathbf{H}^{(l)}(s)$ must be able to represent the frequency response of modal lines described by (6), even for electrically long interconnects where propagation delays are very large. Purely rational approximations, as those generated by vector fitting [3], are ruled out by the possible presence of large delays, which would dramatically increase the required number of poles. We adopt a highly efficient black-box model with delays that has been recently proposed for long scalar lines [14]. This formulation, applied to the above-defined modal lines, reads

$$\mathbf{H}^{(l)}(s) = \frac{\mathbf{N}^{(l)}(s)}{d^{(l)}(s)} = \frac{1}{d^{(l)}(s)} \begin{bmatrix} N_{11}^{(l)}(s) & N_{12}^{(l)}(s) \\ N_{21}^{(l)}(s) & N_{22}^{(l)}(s) \end{bmatrix} \tag{15a}$$

$$N_{pp}^{(l)}(s) = Q_{0p}^{(l)}(s) + Q_{2p}^{(l)}(s)e^{-2s\tau_l}, \qquad p = 1,2 \tag{15b}$$

$$N_{21}^{(l)}(s) = N_{12}^{(l)}(s) = Q_1^{(l)}(s)e^{-s\tau_l} \tag{15c}$$

$$d^{(l)}(s) = q_0^{(l)}(s) + q_2^{(l)}(s)e^{-2s\tau_l} \tag{15d}$$

where τ_l is the time-of-flight of the lth modal line, and the factors $Q_{mp}^{(l)}(s)$, $Q_1^{(l)}(s)$, and $q_m^{(l)}(s)$ are rational coefficients

$$Q_{mp}^{(l)}(s) = \sum_{n=0}^{\bar{n}} R_{mpn}^{(l)}\phi_n(s), \qquad m = 0,2 \tag{16a}$$

$$q_m^{(l)}(s) = \sum_{n=0}^{\bar{n}} r_{mn}^{(l)}\phi_n(s), \qquad m = 0,2 \tag{16b}$$

$$Q_1^{(l)}(s) = \sum_{n=0}^{\bar{n}} R_{1n}^{(l)}\phi_n(s) \tag{16c}$$

defined using the partial fractions basis

$$\phi_n(s) = \begin{cases} 1, & \text{for } n = 0 \\ \frac{1}{s-a_n}, & \text{for } n = 1,\ldots,\bar{n}. \end{cases} \tag{17}$$

The adopted transfer function of (15a)–(15d) mimics the method of characteristics model for a uniform transmission line. It includes a combination of delay operators $e^{-s\tau_l}$ to represent pure propagation, and rational terms to represent nonideal effects like signal dispersion and attenuation. Thanks to the delay operator in the denominator $d^{(l)}(s)$, this formulation represents in a closed form all infinite signal paths due to multiple reflections at line terminations. A small number of poles will be sufficient for the rational terms $Q_{mp}^{(l)}(s)$, $Q_1^{(l)}(s)$, and $q_m^{(l)}(s)$ since fast phase variations induced by propagation delays are explicitly accounted for in the model structure. Therefore, the model complexity is significantly reduced with respect to a purely rational transfer function.

III. Fitting Algorithm

We now describe the main curve-fitting scheme for minimization of the least squares error between the model response and the raw frequency samples (2). We define this error as

$$\mathcal{E}^2 = \sum_{k=1}^{\bar{k}} \|\mathbf{H}(j\omega_k) - \mathbf{H}_k\|_F^2 \tag{18}$$

where $\|\mathbf{A}\|_F$ denotes the Frobenius norm.

A. Estimation of Modal Decomposition Matrix

For interconnects that are not cyclic symmetric, an approximate modal decomposition matrix $\mathbf{R}$ can be estimated from the raw scattering samples (1) with the algorithm described in [22]. The eigendecomposition of $\mathbf{H}_{11,k}$ is computed at each frequency point ω_k as

$$\tilde{\mathbf{R}}_k^H \mathbf{H}_{11,k} \tilde{\mathbf{R}}_k = \tilde{\mathbf{\Lambda}}_{11,k}. \tag{19}$$

The imaginary part of $\tilde{\mathbf{R}}_k$ is minimized by rotating each eigenvector and then discarded. Finally, the result is reorthogonalized using QR decomposition [26]. This procedure leads to a set of possible modal decomposition matrices $\mathbf{R}_k$. Among them, the optimal $\mathbf{R}$ is selected as the matrix $\mathbf{R}_k$ that minimizes the off-diagonal terms in (5).

B. Fitting in Modal Domain

Once the modal decomposition matrix (3) is formed, the modal macromodels $\mathbf{H}^{(l)}(s)$ in (7) can be directly identified from the projected samples (6). Setting

$$\mathbf{\Delta}_k = \mathrm{blkdiag}\left\{\mathbf{H}^{(l)}(j\omega_k)\right\} - \mathbf{H}''_k \tag{20}$$

and substituting (4), (5), and (7) into (18), we can show that[1]

$$\begin{aligned}\mathcal{E}^2 &= \sum_{k=1}^{\bar{k}} \left\|\mathbf{T}\mathbf{P}\mathbf{\Delta}_k\mathbf{P}^T\mathbf{T}^T\right\|_F^2 \\ &= \sum_{k=1}^{\bar{k}} \mathrm{Tr}\left\{\mathbf{T}\mathbf{P}\mathbf{\Delta}_k\mathbf{\Delta}_k^H\mathbf{P}^T\mathbf{T}^T\right\} \\ &= \sum_{k=1}^{\bar{k}} \mathrm{Tr}\left\{\mathbf{\Delta}_k\mathbf{\Delta}_k^H\right\} = \sum_{l=1}^{L}\left(\mathcal{E}^{(l)}\right)^2\end{aligned} \tag{21}$$

where

$$\left(\mathcal{E}^{(l)}\right)^2 = \sum_{k=1}^{\bar{k}} \left\|\mathbf{H}^{(l)}(j\omega_k) - \mathbf{H}_k^{(l)}\right\|_F^2 \tag{22}$$

and $\mathrm{Tr}\{\cdot\}$ denotes the matrix trace. The global fitting error (21) is thus expressed as the sum of the fitting errors between each modal model $\mathbf{H}^{(l)}(s)$ and the corresponding frequency samples (6). As all these error terms depend on separate subsets of unknowns, minimization of $\mathcal{E}^2$ can be performed as L independent tasks, each one minimizing (22), i.e., fitting the model (15a)–(15d) to the corresponding modal line samples (6).

Minimization of (22) is a nonlinear problem in the unknowns of (15d) and in τ_l, which can be solved in principle with nonlinear optimization algorithms of the Newton and quasi-Newton type, like steepest descent, conjugate gradient, Broyden–Fletcher–Goldfarb–Shanno (BFGS) [27]. However, it is well known that these methods can be slow and may stagnate at local minima when applied to this kind of fitting problems. Other approaches that require only the solution of linear least squares problems are preferred in general [3]–[5]. Minimization of (22) is achieved here by an iterative Sanathanan–Koerner fitting algorithm combined with a delay estimation procedure [14].

[1]The trace property $\mathrm{Tr}\{\mathbf{ABC}\} = \mathrm{Tr}\{\mathbf{CAB}\} = \mathrm{Tr}\{\mathbf{BCA}\}$ is used.

C. Delay Estimation

The first step in the minimization of (22) is the estimation of the propagation delay τ_l in (15a)–(15d) from the frequency samples (6). This task can be accomplished in several ways, using either time-frequency decompositions [12], [13], [28], vector fitting [29], or the Hilbert transform [16], [18]. For the purpose of the identification of τ_l in (15a)–(15d), all approaches are feasible, and we adopted [29] because of its simplicity. This algorithm has been applied to the insertion loss samples for the lth modal line $\lambda_{12,k}^{(l)}$, where τ_l appears as the dominant delay.

D. Rational Identification

Once all propagation delays τ_l are known, the model coefficients $R_{mpn}^{(l)}$, $R_{1n}^{(l)}$, and $r_{mn}^{(l)}$ are estimated using a generalization of the Sanathanan–Koerner method [14] that iteratively finds a minimum to the error (22). This procedure is well established in macromodeling [3]–[5], [12], [14], [30]. We, therefore, summarize only its main steps, and point the reader to the references above for more details. Error (22) is rewritten as a function of the numerator and denominator of (15a)–(15d)

$$\left(\mathcal{E}^{(l)}\right)^2 = \sum_{k=1}^{\bar{k}} \left\| \frac{\mathbf{N}^{(l)}(j\omega_k) - d^{(l)}(j\omega_k)\mathbf{H}_k^{(l)}}{d^{(l)}(j\omega_k)} \right\|_F^2. \tag{23}$$

Main difficulty in minimizing (23) is the presence of unknowns in the denominator $d^{(l)}$, which makes this problem nonlinear. The Sanathanan–Koerner iteration [4] overcomes this issue with an iterative process that at each iteration minimizes the linearized error

$$\left(\mathcal{E}_i^{(l)}\right)^2 = \sum_{k=1}^{\bar{k}} \left\| \frac{\mathbf{N}_i^{(l)}(j\omega_k) - d_i^{(l)}(j\omega_k)\mathbf{H}_k^{(l)}}{d_{(i-1)}^{(l)}(j\omega_k)} \right\|_F^2 \tag{24}$$

where subscript i is the iteration counter. Since the denominator of (24) is known from previous iteration (or initialized at one at first iteration), minimization of (24) is a linear least squares problem that can be easily and efficiently solved using QR or singular value decomposition (SVD) [26].

E. Optimizations

The delay-rational identification of Sections III-C and D can be further improved in two ways. First optimization involves a refinement of the modal delay estimates τ_l. An accurate delay estimation is indeed very important since an optimal value can minimize the order $\bar{n}$ of the rational factors in (16a)–(16c), thus improving model accuracy and efficiency. However, a coarse data sampling and/or a restricted measurement bandwidth of (1) can limit the accuracy of all delay estimation algorithms cited in Section III-C because of the fundamental limits set by the time-frequency uncertainty principle [31] and the sampling theorem [32]. In this situation, the initial estimate for τ_l obtained from the raw frequency data can be used to setup an optimization loop that minimizes the fitting error $\mathcal{E}^{(l)}$ by refining τ_l.

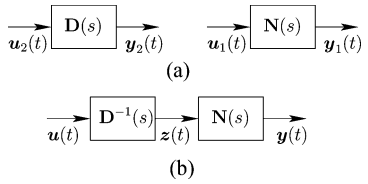

Fig. 2. Graphical illustration of the proposed realization procedure, with notation. (a) Separate realization of numerator and denominator. (b) Inversion of denominator and cascading.

This task, which is not time consuming because only one optimization variable is involved, was performed in all examples of Section VI using the simplex method [33].

A second optimization is possible if the interconnect under investigation is cyclic symmetric, by exploiting the spectral properties of circulant symmetric matrices (11). Since all entries in the projected frequency data (6) satisfy (11), we have

$$\mathbf{H}_k^{(l)} = \mathbf{H}_k^{(L+2-l)}, \qquad l = 2, \ldots, \nu \tag{25}$$

Hence, only the modal macromodels (15a)–(15d) for $l = 1, \ldots, L/2 + 1$ when L is even or $l = 1, \ldots, (L+1)/2$ when L is odd must be identified since

$$\mathbf{H}^{(L+2-l)}(s) = \mathbf{H}^{(l)}(s), \qquad l = 2, \ldots, \nu. \tag{26}$$

Thanks to this observation, the computational cost of the model identification is reduced by a factor that approaches 2 for large L.

IV. Model Realization

An important requirement for black-box macromodels is the possibility to cast them as equivalent electric circuits, compatible with any circuit solver. Circuit synthesis is quite trivial for purely rational macromodels [11] or for models with only delay operators at the numerator [12]. Conversely, a direct synthesis is more difficult for models including delay operators at denominator, as in (15a)–(15d). In this section, we present a sound mathematical procedure to convert transfer functions in the form of (15a)–(15d) into a set of differential equations with delays, thus enabling a straightforward equivalent circuit synthesis. The main result will also play a crucial role in the design of a numerical algorithm to ascertain model stability (see Section V-A).

Among the different terms of the model transfer function (7), synthesis of matrices $\mathbf{P}$ and $\mathbf{T}$ is straightforward since it is achieved with a set of current- or voltage-controlled sources. Main difficulty is instead the realization of the modal macromodels $\mathbf{H}^{(l)}(s)$. Throughout this entire section, we consider a single modal macromodel, dropping the superscript $^{(l)}$ to enhance readability. Realization of (15a)–(15d) involves three steps. First, two separate realizations are derived for the model numerator $\mathbf{N}(s)$ and denominator $\mathbf{D}(s) = d(s)\mathbf{I}_2$ independently. Second, a realization for $\mathbf{D}^{-1}(s)$ is obtained. Finally, the latter is cascaded with the numerator to realize the complete transfer function (15a)–(15d). This process is depicted in Fig. 2.

A. Numerator and Denominator Realizations

The numerator $\mathbf{N}(s)$ and denominator $\mathbf{D}(s)$ defined in (15a)–(15d) and depicted in Fig. 2(a) are the sum of rational terms and exponential delay operators. The rational terms are readily converted into state-space systems using the standard approach documented in [6]. The result is

$$\mathbf{N}(s) = \sum_{m=0}^{2} \left[\mathbf{G}_m(s\mathbf{I} - \mathbf{A})^{-1}\mathbf{B}_0 + \mathbf{L}_m\right] e^{-ms\tau} \tag{27}$$

$$\mathbf{D}(s) = \sum_{m=0,2} \left[\mathbf{F}_m(s\mathbf{I} - \mathbf{A})^{-1}\mathbf{B}_0 + \mathbf{D}_m\right] e^{-ms\tau} \tag{28}$$

where

$$\mathbf{A} = \mathrm{blkdiag}\{a_n\mathbf{I}_2\} \tag{29a}$$

$$\mathbf{B}_0 = [\mathbf{I}_2, \ldots, \mathbf{I}_2]^T \tag{29b}$$

$$\mathbf{G}_m = \begin{bmatrix} R_{m11} & 0 & \cdots & R_{m1\bar{n}} & 0 \\ 0 & R_{m21} & \cdots & 0 & R_{m2\bar{n}} \end{bmatrix}, \qquad m = 0, 2 \tag{29c}$$

$$\mathbf{G}_1 = \begin{bmatrix} 0 & R_{11} & \cdots & 0 & R_{1\bar{n}} \\ R_{11} & 0 & \cdots & R_{1\bar{n}} & 0 \end{bmatrix} \tag{29d}$$

$$\mathbf{L}_m = \begin{bmatrix} R_{m10} & 0 \\ 0 & R_{m20} \end{bmatrix}, \qquad m = 0, 2 \tag{29e}$$

$$\mathbf{L}_1 = \begin{bmatrix} 0 & R_{10} \\ R_{10} & 0 \end{bmatrix} \tag{29f}$$

$$\mathbf{F}_m = [\, r_{m1}\mathbf{I}_2 \quad \cdots \quad r_{m\bar{n}}\mathbf{I}_2 \,], \qquad m = 0, 2 \tag{29g}$$

$$\mathbf{D}_m = r_{m0}\mathbf{I}_2, \qquad m = 0, 2. \tag{29h}$$

By taking the inverse Laplace transform of (27), we obtain a set of delay-differential equations representing numerator $\mathbf{N}(s)$

$$\begin{cases} \dot{\boldsymbol{x}}_1(t) = \mathbf{A}\boldsymbol{x}_1(t) + \mathbf{B}_0\boldsymbol{u}_1(t) \\ \boldsymbol{y}_1(t) = \sum_{m=0}^{2} [\, \mathbf{G}_m \quad \mathbf{L}_m \,] \begin{bmatrix} \boldsymbol{x}_1(t - m\tau) \\ \boldsymbol{u}_1(t - m\tau) \end{bmatrix} \end{cases} \tag{30}$$

where $\boldsymbol{u}_1(t)$ and $\boldsymbol{y}_1(t)$ correspond to input and output of the numerator block, as depicted in Fig. 2(a). Similarly, we have for the denominator $\mathbf{D}(s)$ the realization

$$\begin{cases} \dot{\boldsymbol{x}}_2(t) = \mathbf{A}\boldsymbol{x}_2(t) + \mathbf{B}_0\boldsymbol{u}_2(t) \\ \boldsymbol{y}_2(t) = \sum_{m=0,2} [\, \mathbf{F}_m \quad \mathbf{D}_m \,] \begin{bmatrix} \boldsymbol{x}_2(t - m\tau) \\ \boldsymbol{u}_2(t - m\tau) \end{bmatrix}. \end{cases} \tag{31}$$

A representation of the inverse denominator $\mathbf{D}^{-1}(s)$ is now obtained by exchanging the roles of input $\boldsymbol{u}_2(t)$ and output $\boldsymbol{y}_2(t)$, followed by a simple rearrangement of the terms in (31)

$$\begin{bmatrix} \mathbf{I} & 0 \\ 0 & 0 \end{bmatrix} \begin{bmatrix} \dot{\boldsymbol{x}}_2(t) \\ \dot{\boldsymbol{u}}_2(t) \end{bmatrix} = \begin{bmatrix} \mathbf{A} & \mathbf{B}_0 \\ \mathbf{F}_0 & \mathbf{D}_0 \end{bmatrix} \begin{bmatrix} \boldsymbol{x}_2(t) \\ \boldsymbol{u}_2(t) \end{bmatrix} + \begin{bmatrix} 0 & 0 \\ \mathbf{F}_2 & \mathbf{D}_2 \end{bmatrix} \times \begin{bmatrix} \boldsymbol{x}_2(t - 2\tau) \\ \boldsymbol{u}_2(t - 2\tau) \end{bmatrix} + \begin{bmatrix} 0 \\ -\mathbf{I} \end{bmatrix} \boldsymbol{y}_2(t). \tag{32}$$

B. Cascading

The complete macromodel realization is the cascade of the subsystems representing $\mathbf{D}^{-1}(s)$ and $\mathbf{N}(s)$, as shown in

Fig. 2(b). This is obtained by combining (32) and (30) while enforcing $\boldsymbol{u}_1(t) = \boldsymbol{u}_2(t) = \boldsymbol{z}(t)$. This step leads to the realization

$$\begin{cases} \mathbf{E}'\dot{\boldsymbol{x}}'(t) = \mathbf{A}_0'\boldsymbol{x}'(t) + \mathbf{A}_2'\boldsymbol{x}'(t-2\tau) + \mathbf{B}'\boldsymbol{u}(t) \\ \boldsymbol{y}(t) = \sum_{m=0}^{2} \mathbf{C}_m'\boldsymbol{x}'(t-m\tau). \end{cases} \tag{33}$$

where $\boldsymbol{u}(t) = \boldsymbol{y}_2(t)$ and $\boldsymbol{y}(t) = \boldsymbol{y}_1(t)$ define the macromodel input and output signals, and where

$$\mathbf{E}' = \begin{bmatrix} \mathbf{I} & 0 & 0 \\ 0 & \mathbf{I} & 0 \\ 0 & 0 & 0 \end{bmatrix}$$

$$\mathbf{B}' = \begin{bmatrix} 0 \\ 0 \\ -\mathbf{I} \end{bmatrix} \tag{34a}$$

$$\mathbf{A}_0' = \begin{bmatrix} \mathbf{A} & 0 & \mathbf{B}_0 \\ 0 & \mathbf{A} & \mathbf{B}_0 \\ 0 & \mathbf{F}_0 & \mathbf{D}_0 \end{bmatrix}$$

$$\mathbf{A}_2' = \begin{bmatrix} 0 & 0 & 0 \\ 0 & 0 & 0 \\ 0 & \mathbf{F}_2 & \mathbf{D}_2 \end{bmatrix} \tag{34b}$$

$$\mathbf{C}_m' = [\mathbf{G}_m \quad 0 \quad \mathbf{L}_m]$$

$$\boldsymbol{x}'(t) = [\boldsymbol{x}_1(t) \quad \boldsymbol{x}_2(t) \quad \boldsymbol{z}(t)]^T. \tag{34c}$$

C. Complexity Reduction

Realization (33) is not minimal. Indeed, several uncontrollable states [34] are revealed by applying the following state vector transformation:

$$\boldsymbol{x}''(t) = \mathbf{W}^{-1}\boldsymbol{x}'(t) = \frac{1}{\sqrt{2}} \begin{bmatrix} \boldsymbol{x}_1(t) + \boldsymbol{x}_2(t) \\ \boldsymbol{x}_1(t) - \boldsymbol{x}_2(t) \\ \boldsymbol{z}(t) \end{bmatrix} \tag{35}$$

where

$$\mathbf{W} = \mathbf{W}^{-1} = \frac{1}{\sqrt{2}} \begin{bmatrix} \mathbf{I} & \mathbf{I} & 0 \\ \mathbf{I} & -\mathbf{I} & 0 \\ 0 & 0 & \mathbf{I} \end{bmatrix} \tag{36}$$

and by multiplying the first equation of (33) on the left by $\mathbf{W}^{-1}$. This similarity transformation leads to an equivalent representation of (15a)–(15d) with matrices

$$\mathbf{E}'' = \mathbf{W}^{-1}\mathbf{E}'\mathbf{W} = \begin{bmatrix} \mathbf{I} & 0 & 0 \\ 0 & \mathbf{I} & 0 \\ 0 & 0 & 0 \end{bmatrix}$$

$$\mathbf{B}'' = \mathbf{W}^{-1}\mathbf{B}' = \begin{bmatrix} 0 \\ 0 \\ -\mathbf{I}/\sqrt{2} \end{bmatrix} \tag{37a}$$

$$\mathbf{A}_0'' = \mathbf{W}^{-1}\mathbf{A}_0'\mathbf{W} = \begin{bmatrix} \mathbf{A} & 0 & \mathbf{B}_0 \\ 0 & \mathbf{A} & 0 \\ \mathbf{F}_0/2 & -\mathbf{F}_0/2 & \mathbf{D}_0/2 \end{bmatrix} \tag{37b}$$

$$\mathbf{A}_2'' = \mathbf{W}^{-1}\mathbf{A}_2'\mathbf{W} = \begin{bmatrix} 0 & 0 & 0 \\ 0 & 0 & 0 \\ \mathbf{F}_2/2 & -\mathbf{F}_2/2 & \mathbf{D}_2/2 \end{bmatrix}. \tag{37c}$$

The states corresponding to the second block row in the above matrices are uncontrollable since they are not coupled to the other states by the system dynamics and they are not excited by any input. The second block row and the $(\boldsymbol{x}_1(t) - \boldsymbol{x}_2(t))$ block in $\boldsymbol{x}''(t)$ can, therefore, be removed without affecting the input–output transfer function. As a result, we obtain a more compact realization of (15a)–(15d)

$$\begin{cases} \mathbf{E}\dot{\boldsymbol{x}}(t) = \mathbf{A}_0\boldsymbol{x}(t) + \mathbf{A}_2\boldsymbol{x}(t-2\tau) + \mathbf{B}\boldsymbol{u}(t) \\ \boldsymbol{y}(t) = \sum_{m=0}^{2} \mathbf{C}_m\boldsymbol{x}(t-m\tau) \end{cases} \tag{38}$$

where

$$\mathbf{E} = \begin{bmatrix} \mathbf{I}_{2\bar{n}} & 0 \\ 0 & 0 \end{bmatrix} \qquad \mathbf{B} = \begin{bmatrix} 0 \\ -\mathbf{I}_2 \end{bmatrix} \tag{39a}$$

$$\mathbf{A}_0 = \begin{bmatrix} \mathbf{A} & \mathbf{B}_0 \\ \mathbf{F}_0 & \mathbf{D}_0 \end{bmatrix} \qquad \mathbf{A}_2 = \begin{bmatrix} 0 & 0 \\ \mathbf{F}_2 & \mathbf{D}_2 \end{bmatrix} \tag{39b}$$

$$\mathbf{C}_m = [\mathbf{G}_m \quad \mathbf{L}_m] \quad \boldsymbol{x}(t) = \begin{bmatrix} \boldsymbol{x}_1(t) + \boldsymbol{x}_2(t) \\ \boldsymbol{z}(t) \end{bmatrix}. \tag{39c}$$

This realization is one of the main achievements of this paper, as it enables both a SPICE synthesis and a stability check of proposed model (7).

We note that (38) is in the form of a *descriptor* system with delays [35], differing from *state space* systems because of the matrix $\mathbf{E}$ in front of $\dot{\boldsymbol{x}}(t)$. When $\text{rank}\mathbf{E} < \text{rank}\mathbf{A}$, the system is not fully differential, but includes also algebraic relations.

D. SPICE Synthesis

The conversion of the modal macromodels $\mathbf{H}^{(l)}(s)$, $l = 1, \ldots, L$ into equivalent circuits including only standard (constant) elements is straightforward once (38) is available. Capacitors are used for time derivatives, resistors and controlled sources for multiplication by constants, and matched ideal transmission lines for delay operators [12].

Once separate circuit realizations are available for the modal macromodels, they are connected to the external macromodel ports by a set of constant controlled sources representing the modal profile matrices $\mathbf{TP}$ and $\mathbf{P}^T\mathbf{T}^T$ in (7). Details are omitted here for the sake of brevity. We remark that since only basic circuit elements are used in the synthesis, the proposed circuit realization is intrinsically compatible with any free or commercial circuit solver.

V. Physical Consistency

Physical consistency has been recognized as a crucial requirement for stable and reliable results from transient simulations. In case of lumped models, this consistency amounts to preserving stability, causality, and passivity [36]. These requirements, which are appropriate for standard rational macromodels, are not sufficient to ensure a proper physical behavior for systems in descriptor form (38). This section presents the appropriate generalizations together with a numerical algorithm for checking the physical consistency of the proposed macromodel.

A. Admissibility Test

The descriptor form (38) encompasses a broader class of systems with respect to the standard state space formulation. Besides unstable behavior, it may also include impulsive modes and even a nonunique solution [35]. A stable descriptor system having a unique solution and no impulsive modes is called *admissible* [35]. It turns out that admissibility is the right requirement to make (15a)–(15d) physically consistent. The following theorem [35] gives an algebraic condition to check if the proposed model in its descriptor form (38) is admissible.

Theorem 1: If there exist matrices $\mathbf{P}_1 > 0$, $\mathbf{Q} > 0$, and $\mathbf{Q}_1$ such that

$$\begin{bmatrix} \mathbf{A}_0^T\mathbf{Y} + \mathbf{Y}^T\mathbf{A}_0 + \mathbf{Q} & \mathbf{Y}^T\mathbf{A}_2 \\ \mathbf{A}_2^T\mathbf{Y} & -\mathbf{Q} \end{bmatrix} < 0 \tag{40}$$

where $\mathbf{Y} = \mathbf{P}_1\mathbf{E} + \mathbf{S}\mathbf{Q}_1$ and $\mathbf{S} \in \mathbb{R}^{2\bar{n}+2\times 2}$ is any full column rank matrix satisfying $\mathbf{E}^T\mathbf{S} = 0$, then the system (38) is admissible (hence, stable).

Application of this theorem to system (38) is straightforward since matrix $\mathbf{S}$ can be chosen in closed form as $\mathbf{S} = [\mathbf{0} \quad \mathbf{I}_2]^T$. A main advantage of Theorem 1 is that the admissibility condition is expressed as a set of linear matrix inequalities. Therefore, several well-established algorithms for convex optimization problems, like interior point methods [37], [38], can be used for its solution. In all application examples of Section VI, we solved (40) with SeDuMi [39].

B. Passivity

It is well know that stable, but nonpassive macromodels do not guarantee a stable solution when connected to arbitrary loads, even when the latter are passive [36]. Passivity enforcement of interconnect macromodels has been the subject of intense research over the last few years. Several methods are now available for the detection and the *a-posteriori* correction of passivity violations in the case of purely rational macromodels. We can cite optimal methods based on convex optimization [40] or suboptimal methods based on linear and quadratic programming [41], [42] or eigenvalue perturbation of Hamiltonian matrices [43], [44]. Suboptimal techniques are usually preferred since optimal methods have a very high computational cost for medium to large-size macromodels [45].

Recently, Hamiltonian methods have been extended to models with delays. Good results are available for both pure transmission line models [46]–[48] and for more general black-box models [49] including delay operators only at the numerator. Extension of such techniques to the proposed macromodel structure, with delay operators appearing at the denominator, seems to be feasible given the available theoretical framework. This investigation is outside the scope of this paper and will be presented in a future publication.

VI. Numerical Results

A. Coupled Coplanar Lines

The first example considers a pair of coplanar lines having the cross section depicted in Fig. 3. The interconnect length is set to the very large value of 80 cm in order to demonstrate

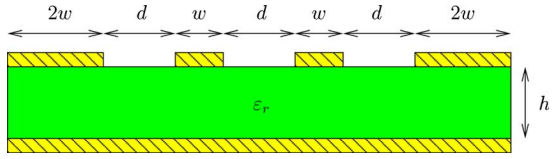

Fig. 3. Cross section of the coupled coplanar lines considered in Section VI-A. Geometrical dimensions are $d = 762\ \mu$m, $w = 381\ \mu$m, and $h = 1193.8\ \mu$m. The thickness of all metal layers is $t = 35.1\ \mu$m. The dielectric has $\varepsilon_r = 4.6$, $\tan\delta = 0.02$, and conductors are made of copper.

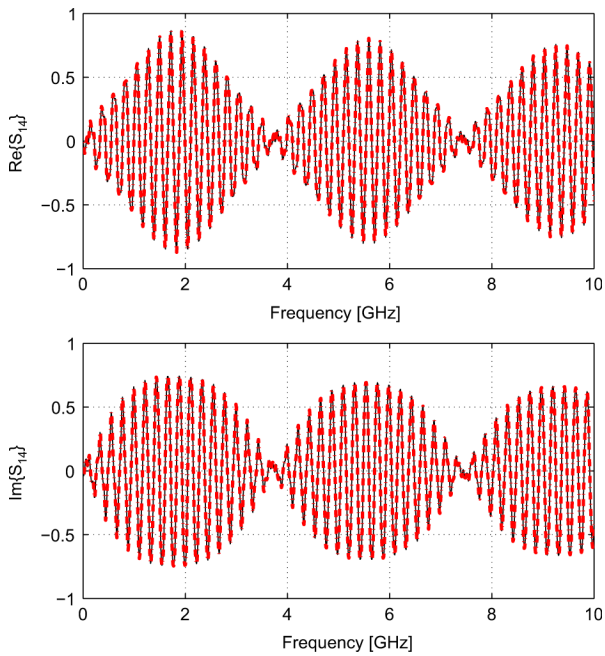

Fig. 4. Comparison of the S_{14} model response (red dashed–dotted line in online version) with the raw data (black solid line) for the coupled coplanar lines. Real (top panel) and imaginary (bottom panel) parts are depicted on a reduced bandwidth to improve readability.

the feasibility of proposed approach. The scattering parameters were computed using IBM EIP tools [50] from 1 kHz up to 40 GHz, and then supplied to the proposed modeling algorithm. A very accurate macromodel was obtained using only 14 poles a_n, as shown in Fig. 4, with a worst case error of 9.3×10^{-3}. The refined model delays turned out to be $\tau_1 = 4.58$ ns and $\tau_2 = 4.33$ ns, and the test of Section V-A proved that the model is well posed, stable, impulse free, and with a unique solution for any given initial condition. Model identification required 610 s, including the delay optimization of Section III-E, and the admissibility check only 1 s.

A comparative test was finally performed between the proposed technique, standard vector fitting, and delayed vector fitting. In order to reach the accuracies reported in Table I, vector fitting required 1500 poles, while delayed vector fitting, needed a combination of 14 poles and six delay elements for each response. Thus, the proposed technique provides a simpler model than all other black-box modeling strategies (vector fitting and delayed vector fitting), while retaining a similar accuracy. Table I also shows that delay-based macromodels provide a better accuracy compared to vector fitting because

TABLE I
MODELING ERROR AND SIMULATION TIME FOR VECTOR FITTING (VF), DELAYED VECTOR FITTING (DVF), METHOD OF CHARACTERISTICS (MoC), AND PROPOSED MACROMODELS OF THE COUPLED COPLANAR LINES OF SECTION VI-A. THE TWO NUMBERS IN THE POLES COLUMN FOR THE MoC MODEL REFER, RESPECTIVELY, TO THE DELAYLESS PROPAGATION OPERATOR AND THE CHARACTERISTIC ADMITTANCE OPERATOR

Method	Poles ($\bar{n}$)	Max error	Sim. time	Speed up
VF	1500	$1.8 \cdot 10^{-2}$	3572 s	-
DVF	14	$7.6 \cdot 10^{-3}$	74.17 s	48x
Proposed	14	$9.3 \cdot 10^{-3}$	8.75 s	408x
MoC	16,10	$3.0 \cdot 10^{-3}$	5.27 s	678x

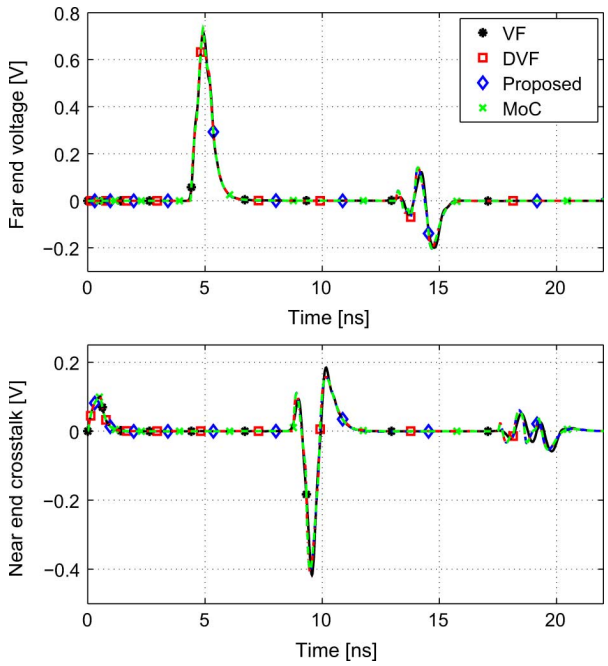

Fig. 5. Far-end (top panel) and near-end (bottom panel) crosstalk predicted using the vector fitting (VF), delayed vector fitting (DVF), method of characteristics (MoC), and proposed macromodels for the coupled coplanar lines.

TABLE II
MODELING ERROR AND SIMULATION TIME FOR VECTOR FITTING (VF), DELAYED VECTOR FITTING (DVF), AND PROPOSED MACROMODELS OF THE DIFFERENTIAL LINK OF SECTION VI-B

Method	Poles ($\bar{n}$)	Max error	Sim. time	Speed up
VF	80	$1.0 \cdot 10^{-2}$	4.66 s	-
DVF	20	$3.0 \cdot 10^{-2}$	8.5 s	0.54x
Proposed	16	$3.2 \cdot 10^{-2}$	1.6 s	2.9x

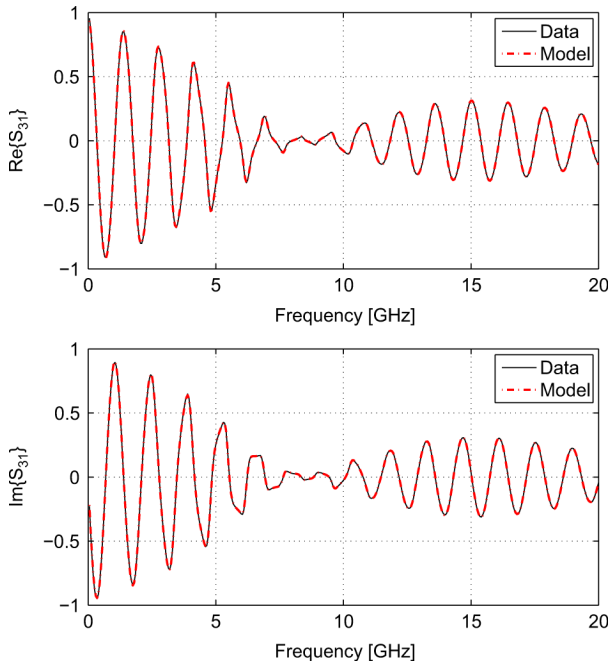

Fig. 6. Comparison of the S_{31} model response (red dashed–dotted line in online version) with the raw data (black solid line) for the differential link of Section VI-B. Real (top panel) and imaginary (bottom panel) part.

of the substantial simplification in the fitting equations to be solved.

The reduced model complexity has a huge impact on the model efficiency, which was tested with a transient simulation using the four different macromodels converted to SPICE format. The line was excited at port 1 by a pulse voltage source (internal resistance 40 Ω, pulsewidth 0.5 ns, rise and fall times 30 ps, peak voltage 1 V), and loaded on ports 2–4 with the parallel of a 3-pF capacitor and a 250-Ω resistor. Table I demonstrates a major improvement in efficiency of the proposed model, with 408× and 8.5× speedup factors with respect to the vector fitting and delayed vector fitting, respectively. The transient simulation results obtained with the different modeling techniques are reported in Fig. 5, showing a very good agreement among all methods.

We now compare our approach with the method of characteristics [2], [20], the most efficient algorithm for modeling uniform cross-section lines starting from per-unit-length parameters. With these assumptions, telegrapher's equations can be used to formulate the macromodel, leading to an optimal model efficiency and accuracy. Comparison with the method of characteristics is, therefore, a challenging benchmark for the proposed macromodel. Table I shows that the performance of the proposed approach are not far from the method of characteristics, a quite remarkable result given the more general and challenging problem addressed in this paper. The identification of the method of characteristics model took only 6.5 s, making this modeling approach clearly preferable for uniform transmission lines. However, the proposed solution gives models of unprecedented efficiency for structures that cannot be modeled with the method of characteristics, as shown in the next three application examples.

B. Differential Printed Circuit Board Stripline

This second example is a 10-cm differential link on a printed circuit board, including two coupled striplines and the corresponding signal launches. This structure is the same considered in the second example of [14], where, however, only a single trace model was computed. Now, thanks to the new theoretical developments, we are able to model the whole four-port S-matrix. Raw scattering data are known from direct measurement over the bandwidth of 0–20 GHz (courtesy of Prof. C. Schuster, formerly with IBM, Yorktown Heights, NY). Due to the moderate interconnect length, this example is a challenging

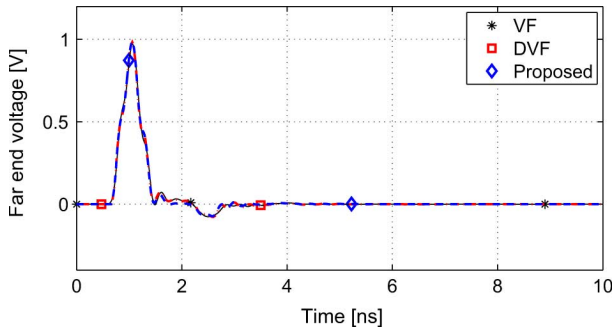

Fig. 7. Far-end voltage for the differential link predicted with vector fitting (VF), delayed vector fitting (DVF), and proposed macromodels.

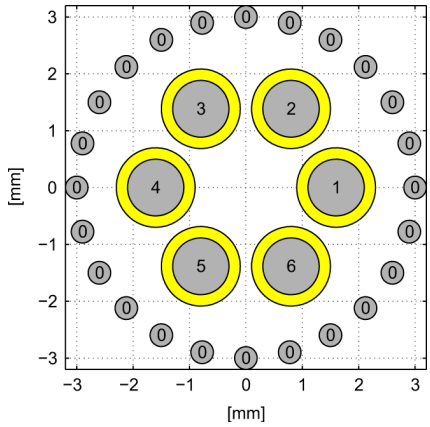

Fig. 8. Cross section of the multiconductor cable of Section VI-C.

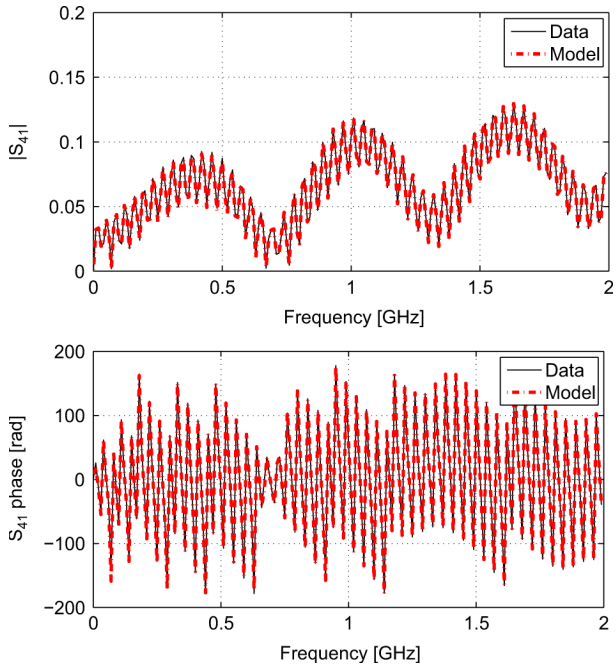

Fig. 9. Comparison of the S_{41} model response (red dashed–dotted line in online version) with the raw data (black solid line) for the multiconductor cable of Section VI-C. Magnitude (top panel), and phase (bottom panel) are shown only up to 2 GHz for readability.

benchmark for the proposed technique since a standard rational vector-fitting model will be a competitive alternative.

Table II reports the number of poles and the corresponding modeling error obtained with vector fitting, delayed vector fitting, and the proposed algorithm. Approximation quality is quite good, especially taking into account that data come from measurement, as can be seen in Fig. 6, where the proposed model insertion loss S_{31} is compared with measured data. The computed modal delays are $\tau_1 = 0.617$ ns and $\tau_2 = 0.66$ ns. The model fulfills all physical consistency requirements of Section V-A, as we proved by solving the linear matrix inequality of Theorem 1. Model identification took 33 s, and the admissibility test required only 1.2 s.

As in the previous example, a transient simulation was performed to assess the model efficiency with respect to vector-fitting and delayed vector-fitting models. A voltage source was applied at port 1 (internal resistance 40 Ω, pulsewidth 0.3 ns, rise and fall time 0.1 ns, peak voltage 1 V). The other ports were terminated into identical passive loads (2.3-nH inductance in series with a parallel *RC* termination with $R = 900\ \Omega$ and $C = 1.5$ pF). Fig. 7 depicts the voltage waveform at port 3, showing good agreement between the results obtained with the three different macromodels. Table II compares the corresponding total simulation times: while delayed vector-fitting model turns out to be less competitive than the rational approximation from vector fitting, the proposed model outperforms vector fitting by almost a factor of 3, which is a remarkable result given the moderate line length. We finally remark that this interconnect cannot be modeled with the method of characteristics because it is not uniform and only the scattering parameters at terminal ports are available.

C. Shielded Multiconductor Cable

Third example is a shielded multiconductor cable of length 2.56 m with six inner signal conductors and an outer shielding layer made by several thin wires. Inner and outer wires are twisted along a helix of step 1 cm in a clockwise and counterclockwise direction, respectively. The diameter is 1 mm for the inner wires and 0.4 mm for the outer wires. The inner and outer conductor circles have radius equal to 1.6 and 3 mm, respectively. Inner conductors are surrounded by a 0.2-mm-thick insulation layer with dielectric constant equal to 4. The background dielectric constant is instead equal to 3. Fig. 8 shows the cable cross section at one end and the lines numbering. The cable S-parameters were computed as follows. First, each step of the helix was divided into 20 sections; each short section was then approximated as a uniform transmission line, and its per-unit-length parameters were computed with the technique described in [51]. Finally, the S-parameters of the cable were computed by cascading the S-matrix of each small section.

The excellent accuracy of the proposed model is shown in Fig. 9, where we intentionally depicted the scattering matrix entry having smallest magnitude; hence, the most sensitive to approximation errors. The worst case modeling error turned out to be equal to 1.0×10^{-2} for a model with $\bar{n} = 14$ poles and delays $\tau_1 = 13.50$ ns, $\tau_2 = \tau_6 = 13.12$ ns, $\tau_3 = \tau_5 = 12.73$ ns, and $\tau_4 = 12.61$ ns. Model identification required 470 s, including the delays optimization described in Section III-E. Delayed vector fitting provided a model of similar accuracy (see Table III), but at the price of a higher complexity, since seven delays per response turned out to be necessary. The excessive

TABLE III
MODELING ERROR AND SIMULATION TIME FOR DELAYED VECTOR FITTING (DVF) AND PROPOSED MACROMODELS OF THE MULTICONDUCTOR CABLE OF SECTION VI-C

Method	Poles ($\bar{n}$)	Max error	Sim. time	Speed up
DVF	14	$2.0 \cdot 10^{-2}$	747.02 s	-
Proposed	14	$1.0 \cdot 10^{-2}$	11.05 s	67.6 x

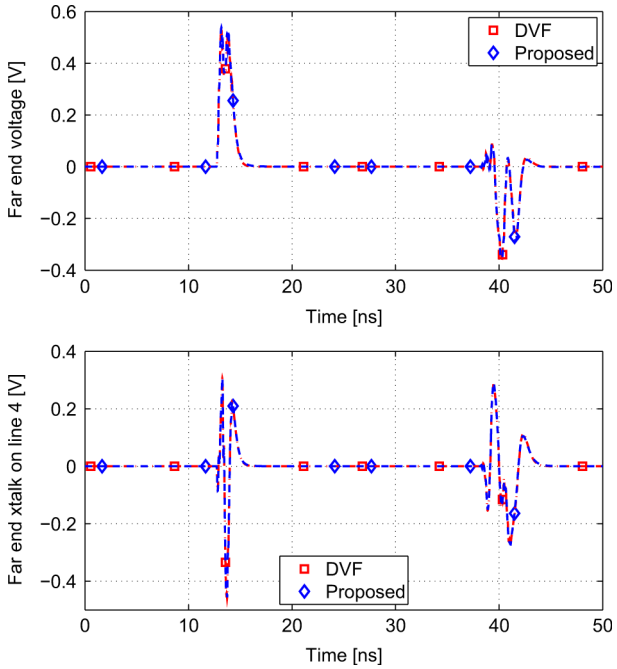

Fig. 10. Far-end voltage (top panel) and far-end crosstalk (bottom panel) for the multiconductor cable of Section VI-C, obtained with the delayed vector fitting (DVF) and the proposed model.

computational cost instead made the generation of a vector-fitting model impossible. The proposed macromodel passed the admissibility check of Section V-A that was solved by SeDuMi in only 7 s.

A comparative transient simulation was finally performed using both macromodels. A voltage pulse (10-Ω internal resistance, 1-nH internal inductance, pulsewidth 0.4 ns, rise and fall time 0.05 ns, peak voltage 1 V) was applied at port 1, while all other ports were terminated into a series 1-nH inductor with a parallel *RC* load ($R = 1.2$ kΩ, $C = 3.3$ pF). Simulation results in Fig. 10 show that delayed vector fitting and proposed macromodels lead to the same waveforms, but with very different computational effort. As reported in Table III, the proposed model is able to cut simulation time by a factor of 67, as compared to delayed vector fitting. Also in this case, the nonuniform cross section impedes the application of the method of characteristics.

D. Ribbon of Microcoaxial Cables

The last example is a ribbon made by four microcoaxial cables having the cross section depicted in Fig. 11. A typical application for these cables is in PDAs, cellphones, and digital cameras, where flexible high-speed connections are needed to connect the main body with the rotating or flipping display unit. The 15-cm line, which is clearly not cyclic symmetric, is made by four signal conductors with diameter 75 μm, each being surrounded by a 100-μm-thick insulation coating (perfluoroalkoxy,

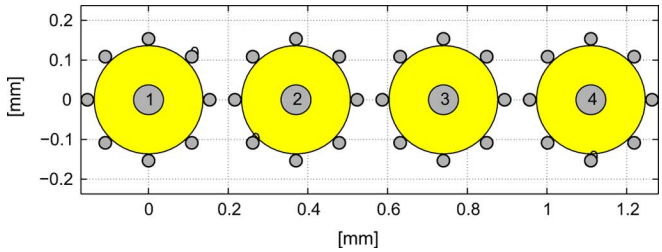

Fig. 11. Cross section of the ribbon cable of Section VI-D.

TABLE IV
MODELING ERROR AND SIMULATION TIME FOR VECTOR FITTING (VF), DELAYED VECTOR FITTING (DVF), AND PROPOSED MACROMODELS OF THE RIBBON CABLE OF SECTION VI-D

Method	Poles ($\bar{n}$)	Max error	Sim. time	Speed up
VF	155	$4.5 \cdot 10^{-3}$	62.6 s	-
DVF	8	$6.8 \cdot 10^{-3}$	16.3 s	3.8 x
Proposed	6	$7.7 \cdot 10^{-3}$	1.7 s	36.8 x

$\varepsilon_r = 2.1$). Each wire is partially shielded by a set of eight small wires (diameter 30 μm), which are twisted along the center wire. Partial shielding is used to cut metal volume and weight. Center-to-center separation between adjacent signal conductors is 0.37 mm.

The per-unit-length parameters of the line were obtained using the algorithm of [51], and the S-parameters of the eight-port interconnect were computed from 0 up to 40 GHz at 2000 linearly spaced points. Modeling was performed with vector fitting, delayed vector fitting, and the proposed technique, leading to the results summarized in Table IV. Since the line is not cyclic symmetric, a frequency-independent modal decoupling matrix $\mathbf{R}$ was obtained from the raw frequency data, as in Section III-A. The estimated matrix turned out to provide a very good decoupling of the original data samples since all off-diagonal terms of (5) had a magnitude below 3.2×10^{-4}. This result thus validates the assumption of a frequency-independent modal decoupling matrix.

The proposed fitting algorithm produced a highly accurate model with a worst case error of 7.7×10^{-3}. Fitting accuracy can be also appreciated on Fig. 12, where the near-end crosstalk $\mathbf{S}_{21}$ is plotted versus the model response. The whole fitting procedure took 370 s, including the delays optimization step, which led to the modal delays $\tau_1 = 0.613$ ns, $\tau_2 = 0.605$ ns, $\tau_3 = 0.617$ ns, and $\tau_4 = 0.615$ ns. Numerical solution of the linear matrix inequality (40) of Section V-A took 2.6 s and certified that the proposed model is admissible. The vector-fitting and delayed vector-fitting models turned out to have larger complexity: vector fitting required 155 poles per response, whereas delayed vector fitting needed eight poles and three delay terms per response.

We finally assess the high efficiency of the proposed model with a transient SPICE simulation. Port 1 was excited by a voltage pulse source (25-Ω internal resistance, 0.8-nH internal inductance, pulsewidth 0.4 ns, rise and fall time 0.05 ns, peak voltage 1 V), with all other ports connected to a 0.8-nH inductor in series with a parallel of a 1-kΩ resistor and a 1.5-pF capacitor. Simulation results obtained with the three macromodels are in good agreement, as shown in Fig. 13. The simulation

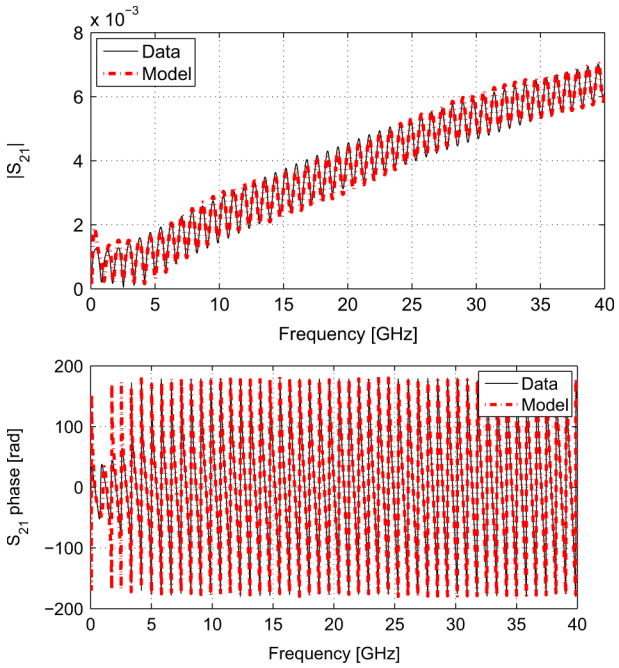

Fig. 12. Comparison of the S_{21} model response (red dashed–dotted line in online versoin) with the raw data (black solid line) for the ribbon cable of Section VI-D. Magnitude (top panel) and phase (bottom panel) are depicted.

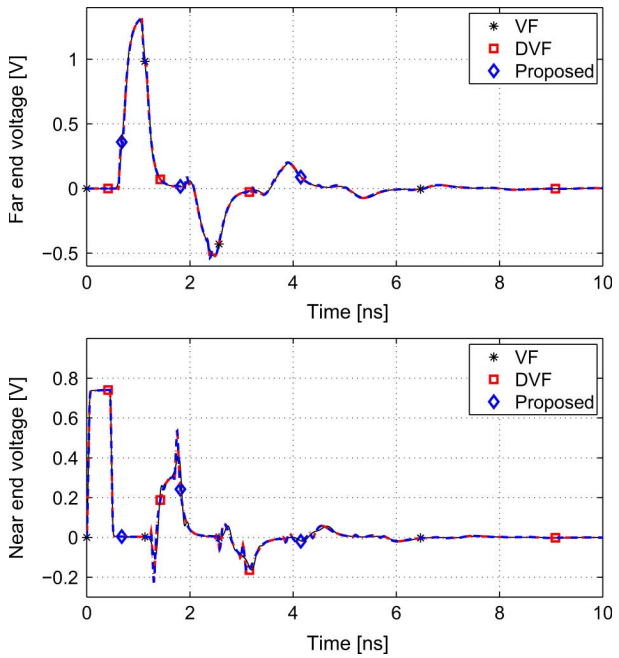

Fig. 13. Far-end (top panel) and near-end (bottom panel) voltage obtained by SPICE simulation of the ribbon cable models returned by vector fitting (VF), delayed vector fitting (DVF), and the proposed algorithm.

times in Table IV confirm the effectiveness of the theoretical developments of this paper since the proposed model outperforms vector fitting by 36.8 times, and delayed vector fitting by 3.8 times.

VII. Conclusion

This paper introduced a novel macromodeling technique for long multiconductor interconnects characterized by tabulated frequency data. This method is able to directly synthesize all infinite delays due to multiple reflections. A formal description of model identification, stability certification, and equivalent-circuit synthesis has been presented.

Several application examples demonstrate the accuracy and robustness of the proposed algorithms and the remarkable efficiency of the proposed model that clearly outperforms more standard solutions. Future research will address model passivity qualification and extension to the more challenging case of frequency-dependent modal profiles.

References

[1] R. Achar and M. Nakhla, "Simulation of high-speed interconnects," *Proc. IEEE*, vol. 89, no. 5, pp. 693–728, May 2001.

[2] C. Paul, *Analysis of Multiconductor Transmission Lines*. New York: Wiley, 1994.

[3] B. Gustavsen and A. Semlyen, "Rational approximation of frequency domain responses by vector fitting," *IEEE Trans. Power Del.*, vol. 14, no. 3, pp. 1052–1061, Jul. 1999.

[4] C. K. Sanathanan and J. Koerner, "Transfer function synthesis as a ratio of two complex polynomials," *IEEE Trans. Autom. Control*, vol. AC-9, no. 1, pp. 56–58, Jan. 1963.

[5] D. Deschrijver, B. Haegeman, and T. Dhaene, "Orthonormal vector fitting: A robust macromodeling tool for rational approximation of frequency domain responses," *IEEE Trans. Adv. Packag.*, vol. 30, no. 2, pp. 216–225, May 2007.

[6] S. Grivet-Talocia and A. Ubolli, "On the generation of large passive macromodels for complex interconnect structures," *IEEE Trans. Adv. Packag.*, vol. 29, no. 1, pp. 39–54, Feb. 2006.

[7] R. Araneo, "Extraction of broad-band passive lumped equivalent circuits of microwave discontinuities," *IEEE Trans. Microw. Theory Tech.*, vol. 54, no. 1, pp. 393–401, Jan. 2006.

[8] Y. T. Kuo, H. Y. Chao, and Y. Li, "Automatic generation of passive equivalent circuits for broadband microstrip antennas," in *IEEE AP-S Int. Symp.*, Honolulu, HI, Jun. 2007, pp. 3904–3907.

[9] C. K. Liao, C. Y. Chang, and J. Lin, "A vector-fitting formulation for parameter extraction of lossy microwave filters," *IEEE Microw. Wireless Compon. Lett.*, vol. 17, no. 4, pp. 277–279, Apr. 2007.

[10] R. Neumayer and W. Weigel, "Network-parameter-based modeling in microwave design," in *15th Int. Microw., Radar, Wireless Commun. Conf.*, Warsaw, Poland, Jun. 2004, vol. 3, pp. 795–798.

[11] G. Antonini, "SPICE equivalent circuits of frequency-domain responses," *IEEE Trans. Electromagn. Compat.*, vol. 45, no. 8, pp. 502–512, Aug. 2003.

[12] A. Chinea, P. Triverio, and S. Grivet-Talocia, "Delay-based macromodeling of long interconnects from frequency-domain terminal responses," *IEEE Trans. Adv. Packag.*, to be published.

[13] A. Chinea, P. Triverio, and S. Grivet-Talocia, "Compact macromodeling of electrically long interconnects," in *Proc. 17th Top. Elect. Perform. Electron. Packag. Meeting*, San Jose, CA, Oct. 2008, pp. 199–202.

[14] P. Triverio, S. Grivet-Talocia, and A. Chinea, "Black-box identification of delay-based macromodels from measured terminal responses," in *Proc. 13th IEEE Signal Propag. Interconnects Workshop*, Strasbourg, France, May 2009, pp. 1–4.

[15] A. Charest, D. Saraswat, M. Nakhla, R. Achar, and N. Soveiko, "Compact macromodeling of high-speed circuits via delayed rational functions," *IEEE Microw. Wireless Compon. Lett.*, vol. 17, no. 12, pp. 828–830, Dec. 2007.

[16] R. Mandrekar and M. Swaminathan, "Causality enforcement in transient simulation of passive networks through delay extraction," in *9th IEEE Signal Propag. Interconnects Workshop*, Garmisch-Partenkirchen, Germany, May 10–13, 2005, pp. 25–28.

[17] A. Charest, R. Achar, M. Nakhla, and I. Erdin, "Delay extraction-based passive macromodeling techniques for transmission line type interconnects characterized by tabulated multiport data," *Analog Integr. Circuits Signal Process.*, vol. 60, no. 1, pp. 13–25, Aug. 2009.

[18] R. Mandrekar and M. Swaminathan, "Delay extraction from frequency domain data for causal macro-modeling of passive networks," in *IEEE Int. Circuits Syst. Symp.*, May 23–26, 2005, vol. 6, pp. 5758–5761.

[19] A. Charest, M. Nakhla, R. Achar, D. Saraswat, N. Soveiko, and I. Erdin, "Time domain delay extraction-based macromodeling algorithm for long-delay networks," *IEEE Trans. Adv. Packag.*, to be published.

[20] S. Grivet-Talocia, H. Huang, A. Ruehli, F. Canavero, and I. Elfadel, "Transient analysis of lossy transmission lines: An efficient approach based on the method of characteristics," *IEEE Trans. Adv. Packag.*, vol. 27, no. 1, pp. 45–56, Feb. 2004.
[21] N. Nakhla, A. Dounavis, R. Achar, and M. Nakhla, "DEPACT: Delay extraction-based passive compact transmission-line macromodeling algorithm," *IEEE Trans. Adv. Packag.*, vol. 28, no. 1, pp. 13–23, Feb. 2005.
[22] B. Gustavsen, "Fast delay-less interconnect macromodeling and simulation by assumption of a constant eigenvector matrix," in *Proc. 12th IEEE Signal Propag. Interconnects Workshop*, May 12–15, 2008, pp. 1–4.
[23] P. J. Davis, *Circulant Matrices*. New York: Wiley, 1979.
[24] R. Bellman, *Introduction to Matrix Analysis*. New York: McGraw-Hill, 1970.
[25] S. Hovd and M. Skogestad, "Control of symmetrically interconnected plants," *Automatica*, vol. 30, no. 6, pp. 957–973, Jun. 1994.
[26] G. Golub and C. Van Loan, *Matrix Computations*. Baltimore, MD: Johns Hopkins Univ. Press, 1996.
[27] D. Luenberger, *Linear and Nonlinear Programming*. Berlin, Germany: Springer, 2003.
[28] S. Grivet-Talocia, "Delay-based macromodels for long interconnects via time-frequency decompositions," in *Proc. IEEE 15th Elec. Perform. Electron. Packag., Top. Meeting*, Scottsdale, AZ, Oct. 2006, pp. 199–202.
[29] B. Gustavsen, "Time delay identification for transmission line modeling," in *8th IEEE Signal Propag. Interconnects Workshop*, Hildesheim, Germany, May 2004, pp. 103–106.
[30] P. Triverio, M. Nakhla, and S. Grivet-Talocia, "Parametric macromodeling of multiport networks from tabulated data," in *16th Elect. Perform. Electron. Packag. Top. Meeting*, Atlanta, GA, Oct. 29–31, 2007, pp. 51–54.
[31] K. Gröchenig, *Foundations of Time-Frequency Analysis*. Berlin, Germany: Birkhauser, 2001.
[32] A. Jerri, "The Shannon sampling theoremits various extensions and applications: a tutorial review," *Proc. IEEE*, vol. 65, no. 11, pp. 1565–1596, Nov. 1977.
[33] J. Nelder and R. Mead, "A simplex method for function minimization," *Comput. J.*, vol. 7, no. 4, pp. 308–313, Jan. 1965.
[34] K. Zhou, J. Doyle, and K. Glover, *Robust and Optimal Control*. New York: Prentice-Hall, 1996.
[35] S. Xu and J. Lam, *Robust Control and Filtering of Singular Systems*, ser. Lecture Notes Contr. Inform. Sci. Berlin, Germany: Springer, 2006.
[36] P. Triverio, S. Grivet-Talocia, M. S. Nakhla, F. Canavero, and R. Achar, "Stability, causality, and passivity in electrical interconnect models," *IEEE Trans. Adv. Packag.*, vol. 30, no. 4, pp. 795–808, Nov. 2007.
[37] Y. Nesterov and A. Nemirovskii, *Interior-Point Polynomial Algorithms in Convex Programming*. Philadelphia, PA: SIAM, 1994.
[38] S. Boyd and L. Vandenberghe, *Convex Optimization*. Cambridge, U.K.: Cambridge Univ. Press, 2004.
[39] J. Sturm, "Using SeDuMi 1.02, a MATLAB toolbox for optimization over symmetric cones," *Optim. Methods Softw.*, vol. 11, no. 1, pp. 625–653, Jan. 1999.
[40] C. Coelho, J. Phillips, and L. Silveira, "A convex programming approach for generating guaranteed passive approximations to tabulated frequency-data," *IEEE Trans. Comput.-Aided Design Integr. Circuits Syst.*, vol. 23, no. 2, pp. 293–301, Feb. 2004.
[41] B. Gustavsen and A. Semlyen, "Enforcing passivity for admittance matrices approximated by rational functions," *IEEE Trans. Power Syst.*, vol. 16, no. 1, pp. 97–104, Feb. 2001.
[42] D. Saraswat, R. Achar, and M. Nakhla, "Global passivity enforcement algorithm for macromodels of interconnect subnetworks characterized by tabulated data," *IEEE Trans. Very Large Scale Integration (VLSI) Syst.*, vol. 13, no. 7, pp. 819–832, Jul. 2005.
[43] S. Grivet-Talocia, "Passivity enforcement via perturbation of Hamiltonian matrices," *IEEE Trans. Circuits Syst. I, Reg. Papers*, vol. 51, no. 9, pp. 1755–1769, Sep. 2004.
[44] S. Grivet-Talocia and A. Ubolli, "Passivity enforcement with relative error control," *IEEE Trans. Microw. Theory Tech.*, vol. 55, no. 11, pp. 2374–2383, Nov. 2007.
[45] S. Grivet-Talocia and A. Ubolli, "A comparative study of passivity enforcement schemes for linear lumped macromodels," *IEEE Trans. Adv. Packag.*, vol. 31, no. 4, pp. 673–683, Nov. 2008.
[46] E. Gad, C. Chen, M. Nakhla, and R. Achar, "Passivity verification in delay-based macromodels of electrical interconnects," *IEEE Trans. Circuits Syst. I, Reg. Papers*, vol. 52, no. 11, pp. 2173–2187, Nov. 2005.
[47] A. Chinea and S. Grivet-Talocia, "A passivity enforcement scheme for delay-based transmission line macromodels," *IEEE Microw. Wireless Compon. Lett.*, vol. 17, no. 8, pp. 562–564, Aug. 2007.
[48] A. Chinea and S. Grivet-Talocia, "Perturbation schemes for passivity enforcement of delay-based transmission line macromodels," *IEEE Trans. Adv. Packag.*, vol. 31, no. 3, pp. 568–578, Aug. 2008.
[49] A. Charest, M. Nakhla, R. Achar, and C. Chen, "Passivity verification and enforcement of delayed rational function macromodels from networks characterized by tabulated data," in *Proc. 13th Signal Propag. Interconnets Workshop*, Strasbourg, France, May 2009, pp. 1–4.
[50] Electromagnetic Field Solver Suite of Tools. IBM, Armonk, NY, 2009. [Online]. Available: http://www.alphaworks.ibm.com/tech/eip
[51] D. De Zutter and L. Knockaert, "Skin effect modeling based on a differential surface admittance operator," *IEEE Trans. Microw. Theory Tech.*, vol. 53, no. 8, pp. 2526–2538, Aug. 2005.

Piero Triverio (S'06–M'09) received the M.Sc. and Ph.D. degrees in electronics engineering from the Politecnico di Torino, Turin, Italy, in 2005 and 2009, respectively.

He is currently a Research Assistant with the Electromagnetic Compatibility Group, Politecnico di Torino. In 2005 and 2007, he visited the Computer-Aided Engineering Group, Carleton University, Ottawa, ON, Canada. His research interests concern numerical methods for signal integrity and electromagnetic compatibility analysis.

Dr. Triverio was the recipient of the 2007 Best Paper Award of the IEEE TRANSACTIONS ON ADVANCED PACKAGING, the Best Paper Award of the IEEE 17th Topical Meeting on Electrical Performance of Electronic Packaging, and the Best Student Paper Award of the IEEE 15th Topical Meeting on Electrical Performance of Electronic Packaging.

Stefano Grivet-Talocia (M'98–SM'07) received the Laurea and Ph.D. degrees in electronic engineering from the Politecnico di Torino, Turin, Italy.

From 1994 to 1996, he was with the National Aeronautics and Space Administration (NASA)/Goddard Space Flight Center, Greenbelt, MD, where he was involved with applications of fractal geometry and wavelet transform to the analysis and processing of geophysical time series. He is currently an Associate Professor of circuit theory with the Department of Electronics, Politecnico di Torino. He has authored or coauthored over 90 journal and conference papers. His current research interests are passive macromodeling of lumped and distributed interconnect structures, modeling and simulation of fields, circuits, and their interaction, wavelets, time-frequency transforms, and their applications.

Dr. Grivet-Talocia was an associate editor for the IEEE TRANSACTIONS ON ELECTROMAGNETIC COMPATIBILITY (1999–2001). He was corecipient of the 2007 Best Paper Award of the IEEE TRANSACTIONS ON ADVANCED PACKAGING and the IBM Shared University Research (SUR) Award (2007, 2008).

Alessandro Chinea received the Laurea Specialistica (M.Sc.) degree in electronic engineering from the Politecnico di Torino, Turin, Italy, in 2006, and is currently working toward the Ph.d. degree at the Politecnico di Torino.

In 2006, he joined the Electromagnetic Compatibility (EMC) Group, Politecnico di Torino, where he is currently a doctoral student. His research interests concern macromodeling of electrical interconnects for EMC and signal integrity (SI) problems. In particular, he is involved with algorithm development for passivity check and enforcement of distributed models.

Mr. Chinea was the recipient of the Optime Award presented by the Unione Industriale di Torino. He was selected for the IBM EMEA Best Student Recognition Event 2006.